Sensors & Actuators: B. Chemical 400 (2024) 134904

Contents lists available at ScienceDirect

Sensors and Actuators: B. Chemical

journal homepage: www.elsevier.com/locate/snb

Optical hydrogen peroxide sensor for measurements in flow

Anders Ø. Tjell [a], Barbara Jud [a], Roland Schaller-Ammann [b], Torsten Mayr [a,*,1]

[a] Institute of Analytical Chemistry and Food Chemistry, Graz University of Technology, Stremayrgasse 9/II, 8010 Graz, Austria
[b] HEALTH – Institute for Biomedical Research and Technologies, Joanneum Research Forschungsgesellschaft m.b.H, Neue Stiftingtalstraße 2, 8010 Graz, Austria

ARTICLE INFO

Keywords:
Hydrogen peroxide sensor
H_2O_2
Optical sensor
Flow-chemistry
Microfluidic
Flow-through cell

ABSTRACT

An optical hydrogen peroxide (H_2O_2) sensor is presented. The sensor is based on catalytic degradation of H_2O_2 and the detection of produced oxygen (O_2) with a phosphorescent sensor. A novel aspect of the sensor is removal O_2 from the analyte solution in flow. This allows the use of a more sensitive O_2 sensor. Thereby, a better resolution at lower H_2O_2 concentrations is achieved. Sensor spots are integrated in a flow-through cell, and H_2O_2 is measured in flow between 10 and 80 μL/min. The catalytic activities of previously reported catalyst are tested. RuO_2 and silica supported platinum nanoparticles are applied in the sensor with limit of detections of 0.16 and 0.17 μM H_2O_2, respectively. The sensor can measure reliably between 1 and 200 μM H_2O_2. The concentration range can be extended to 1000 μM H_2O_2 by exchanging the O_2 sensor. Interfering species (NaONOO, NaOCl, t-BuOOH, and ascorbic acid) are tested and show only minor cross-sensitivities. The sensor is applied at-line in a model batch reactor with glucose oxidase to showcase production of H_2O_2 from glucose.

1. Introduction

The interest of monitoring Hydrogen peroxide (H_2O_2) is increasing in a variety of different application fields, such as, wastewater treatment [1,2], enzymatic reactions in bioreactors [3–5], and industrial bleaching [6]. In biology, it is related to ageing [7–9], signaling and stress response [10], or human immune response [11], as a reactive oxygen species. Thus, the need for reliable H_2O_2 detection is also increasing.

A common way of detecting H_2O_2 is by employing an assay. However, assays tend to be time consuming and require sampling. Examples of enzymatic assays for H_2O_2 are horseradish peroxidase (HRP) in combination with either 3,5,3′,5′-tetra-methylbenzidine [12] or Amplex Red [13].

Another way to detect H_2O_2 is flow injection analysis systems. They are usually based on chemiluminescent reactions, and most commonly employed are luminol or acridinium ester [14]. Both substances have cross-sensitivities that are reported elsewhere [15,16]. An inherent disadvantage of flow injection analysis is the mixing of chemicals to generate a measurable signal, thereby excluding the possibility to 'reuse' analyte solution. Furthermore, flow injection analysis can be relatively expensive regarding instrumentation and chemicals (depending on the applied reaction). A better option to continuously monitor H_2O_2 is with sensors.

In general, there are two measurement principles for H_2O_2 sensors, namely electrochemical and optical. Electrochemical sensors measure oxidation or reduction of H_2O_2 at the surface of an electrode [17–19]. Oxidation of H_2O_2 releases an electron at the anode, and reduction of H_2O_2 needs to receive an electron from the cathode. A common challenge with electrochemical H_2O_2 sensors is the lack of selectivity, due to a relatively high potential applied. This also causes reaction of other electrochemically active species, e.g., ascorbic acid or uric acid [18,20]. Hence, a lot of research has been carried out on both electrodes and electrocatalysts related to electrochemical H_2O_2 sensing [17,19].

The measurement principle for optical sensor is most commonly based on a change in photophysical properties of an indicator dye when it comes in contact with an analyte, e.g·H_2O_2. Optical indicator dyes for direct H_2O_2 measurement typically lack reversibility, since they are based on an oxidation reaction with H_2O_2. Consequently, both luminescent dyes [21] and nanoparticle based systems [22], are not suited for use as a sensor. Alternatively, O_2 can function as mediating species for indirect H_2O_2 sensing. Optical O_2 sensors are reversible, fast responding, and have tuneable dynamic ranges depending on indicator and immobilization [23,24]. They can function as H_2O_2 sensors by addition of a catalyst, such as catalase, that activates the reaction of H_2O_2 into H_2O and O_2. In general, enzyme based sensors stand out due to high selectivity, but they have other drawbacks, such as complicated

* Corresponding author.
E-mail address: torsten.mayr@tugraz.at (T. Mayr).
[1] ORCID: 0000-0002-7946-585X

https://doi.org/10.1016/j.snb.2023.134904
Received 19 September 2023; Received in revised form 31 October 2023; Accepted 1 November 2023
Available online 4 November 2023

immobilization procedures, susceptibility to pH, long-term stability issues, and potential high cost [17,25].

The concept of optical sensors which are indirectly measuring H_2O_2 based on O_2 indicators was first published with silver powder or catalase as catalyst in 1989 [26]. Since then, other inorganic catalysts have been reported to improve the sensing concept, for instance, manganese dioxide, platinum, or silver [27], ruthenium dioxide [28], and silica supported platinum nanoparticles (PtNP) [29]. To our knowledge, the sensor with PtNP has the lowest reported limit of detection (LOD), at 15 μM H_2O_2, for this H_2O_2 sensing concept.

There are a lot of options for optical detection of O_2, and both sensors and optical indicators have been thoroughly described elsewhere [24,30–32]. Optical oxygen sensors work better at lower concentrations due to the phosphorescence quenching mechanism. Therefore, measuring very small amounts of produced oxygen at air saturation is not feasible. However, smaller concentrations of H_2O_2 can be detected by removing the dissolved oxygen (DO) from the analyte solution and shifting the measurement range to low O_2 concentration.

Here we present an H_2O_2 sensor based on measuring produced O_2 from catalytic degradation of H_2O_2. To improve the sensor, we employ a fluidic set-up to remove DO from the analyte solution, making it possible to utilize an O_2 trace sensor. We further demonstrate the application of the sensor to detect biocatalytic production of H_2O_2 in a model batch reactor.

2. Experimental section

A detailed description of materials and instrumentation can be found in the ESI.

Platinum(II)-6,13,20,27-tetrakis(4-fluorophenyl)tetrabenzoporphyrin and palladium(II)-6,13,20,27-tetrakis(4-fluorophenyl) tetrabenzoporphyrin (PtTPTBPF and PdTPTBPF, respectively) indicators were synthesized in house as previously described [33]. PS/DVB beads were purchased from Sigma Aldrich and stained following a previously published procedure [34]. Sensor read-outs were performed with phase fluorimeters (Firesting O2 or Pico-O2, Pyroscience GmbH, Germany) further equipped with a temperature sensor (PT100, Pyroscience GmbH, Germany). The temperature sensor was placed in close proximity to the flow-through cell to allow temperature compensation of the O_2 measured. Temperature measurements inside the flow-through cell was performed with self-adhesive temperature sensor spots (TPSP5-ADH, Pyroscience GmbH, Germany).

Microfluidic flow-through cells were obtained from Joanneum Research (Graz, Austria) [35]. Poly(ethylene glycol terephthalate) (PET, Mylar®) from Goodfellow, USA. Hydromed™ D7 (D7) from AdvanSource Biomaterials, USA. Silicone tubing (ID = 0.5 mm, OD = 2.5 mm) from microfluidic chipshop, Germany. PEEK tubing (ID = 0.03 in, OD = 1/16 in) from Sigma Aldrich. Ruthenium (IV) oxide hydrate is abbreviated RuO_2.

2.1. Synthesis of PtNP

Fibrous nanosilica supported platinum nanoparticles (PtNP) were synthesized following a previously reported procedure [29]. Details can be found in the ESI.

2.2. Preparation of sensor formulations and foils

The optical sensors were prepared from liquid sensor formulations. For O_2 sensors, the formulation was a solution of either 2% PtTPTBPF or 2% PdTPTBPF indicator immobilized on PS/DVB beads dispersed in 7% D7 in 9:1 EtOH/H_2O. H_2O_2 sensors were prepared by adding 20 mg/mL RuO_2 or 60 mg/mL PtNP to the O_2 sensor formulation. Sensor foils were prepared by knife coating the sensor formulations on a PET support with a 3 MIL bar corresponding to approx. 75 μm wet film.

2.3. Measurement set-up for H_2O_2

Sensor foils were cut out and glued into the flow-through cell with double sided adhesive tape, as can be seen in Fig. 1C. Then, a 2-point O_2 calibration was performed with PBS and 2% Na_2SO_3 before closing the cell with pressure sensitive adhesive tape (ThermalSeal RTS™, Excel Scientific, Inc., USA) and PET foil/double sided tape on top. The inlet and outlet were connected to the microfluidic set-up with commercially available nuts and ferrules (Upchurch Scientific™). The cell was washed with a continuous flow of PBS to remove residue Na_2SO_3.

Oxygen was removed from the sample solution with a set-up as sketched in Fig. 1A. A peristaltic pump (MINIPULS 3, Gilson, USA) was used to control the flow of the analyte solution that was passed through a silicone tube (length 30 cm, ID 0.5 cm) immersed in an oxygen scavenging solution (2% Na_2SO_3). Silicone has a high permeability to oxygen, and oxygen was removed from the analyte solution by diffusing into the oxygen scavenging solution. PEEK tubing was used to connect the silicone tubing to the flow-through cell to minimize reoxygenation after exiting the O_2 scavenging solution. The total volume from the inlet of the set-up to the sensor spot was approx. 135 μL. In the flow-through cell the first sensor spot was for O_2 reference and the second for H_2O_2.

Prior to use, the sensor was conditioned in flow overnight to remove residual oxygen. Calibrations were performed with 100 mM PBS and fresh stock solutions prepared by diluting 30% H_2O_2. Values for calibration curves are obtained from response curves as averages over one minute at a stable signal.

2.4. GOx model batch reactor

10.3 mg glucose oxidase cross-linked enzyme aggregates (GOx-CLEA) was dispersed in 1 mL 7% D7 in 1:9 H_2O/EtOH with a bead mill (Bead Ruptor 4, Omni International, USA), 7 glass beads, speed 3, time 3 min, and then knife coated on a PET foil with a 4 MIL bar. After drying, a 5.7 by 3.7 cm^2 piece was used to cover the inside of a 10 mL vial, which was used as a model batch reactor that was further equipped with an O_2 microsensor, O_2 bubbling, and a magnetic stir bar. The sensor was conditioned overnight with 100 mM PBS in a recirculating set-up to keep the volume constant. 10 or 20 μL 200 mM glucose was added to initiate H_2O_2 production from respectively 200 or 400 μM glucose. The concentration of H_2O_2 was validated with a horseradish peroxidase/Amplex Red (HRP/AR) assay. Samples were stored at −18 °C before conducting the assay or measured directly after sampling.

2.5. HRP/AR assay

A 100 μM Amplex Red (AR) solution was prepared by dissolving 0.52 mg of the indicator in 2 mL DMSO and further diluting to 20 mL with 100 mM PBS. 8.1 mg HRP was dissolved in 1.492 mL 100 mM PBS to achieve a concentration of 5.43 mg/mL. The assay was performed with 25 μM AR, 0.05 U HRP, and 50 μL H_2O_2 solution in a total volume of 3 mL and reaction time 15 min. The H_2O_2 solution was diluted if the measured value was above the calibration range. The fluorescence of the formed resorufin was measured with a fluorescence spectrophotometer Ex 540 nm, Em 550–750 nm (peak 590 nm), Ex slit 5 nm, Em slit 5 nm, and PMT voltage 635 V.

3. Results and discussion

The sensing principle and set-up can be seen in Fig. 1A. H_2O_2 is catalytically degraded inside the H_2O_2 sensor spot, and the amount of produced O_2 is measured. Both an inorganic catalyst and the O_2 sensor beads are immobilized in a polyurethane based hydrogel. In this work, we mainly use red light excitable PdTPTBPF, due to its high sensitivity at low DO concentrations, with an optimal working range between 0% and 5% DO [33,36]. A low level of DO is achieved with the fluidic set-up, where DO is removed from the analyte solution by passing it through

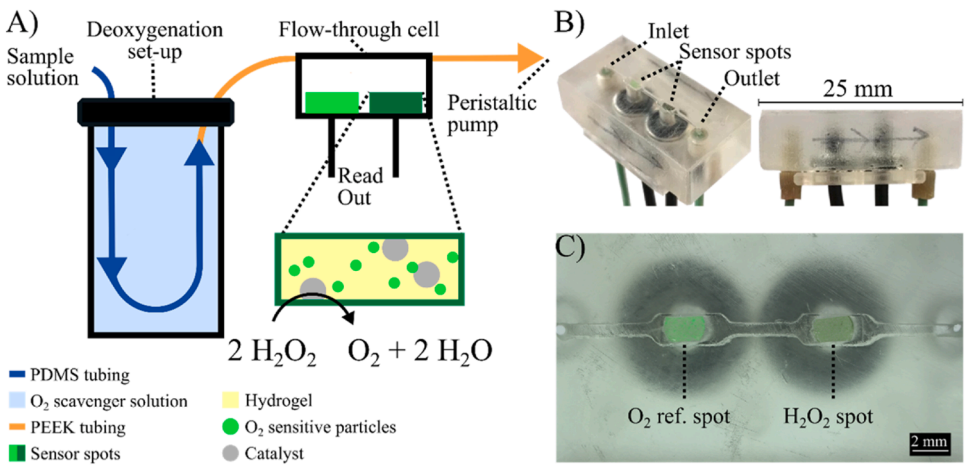

Fig. 1. A) Illustration of the sensor set-up. First, the analyte solution is passed through a silicone tubing submerged in an O_2 scavenging solution, and afterwards H_2O_2 is determined by measuring the amount of produced O_2. O_2 is measured with a sensor spot (light green) consisting of O_2 sensitive particles immobilized in a hydrogel. H_2O_2 is measured with a sensor spot (dark green) containing O_2 sensitive particles and catalyst. The sensor spots are immobilized in a microfluidic flow-through cell, and read-out is performed through optical fibres. B) Photographs of the flow-through cell. C) Sensor spots in the flow-through cell, (left) 'O_2 ref.' and (right) 'H_2O_2'. A picture of the entire set-up can be seen in Fig. S2.

a high gas permeable silicone tube immersed into an O_2 scavenging solution.

3.1. Evaluation of catalysts for H_2O_2 degradation

A key aspect of the sensor is the ability of the catalyst to generate O_2 from H_2O_2, and the activity of the catalyst becomes increasingly more important at lower H_2O_2 concentrations. Several catalysts were investigated, and Fig. 2 shows the production of O_2 at 50 mM H_2O_2 and a catalyst concentration of 0.05 mg/mL for MnO_2, RuO_2, and PtNP. Additionally, catalase and silver powder were also measured. Silver powder produces 0.00137 ± 0.00003 mol min^{-1} g^{-1} and catalase produces 2.46 ± 0.15 mol min^{-1} g^{-1}. Though, it should be noted that catalase dissolves, whereas the inorganic catalysts disperse. Furthermore, it is expected that immobilization of the enzyme in a sensor foil decreases its activity [37].

The reaction kinetics of MnO_2, RuO_2, and PtNP were investigated similar to Michaelis-Menten kinetics for a better comparison. A summary can be seen in Table S1. The reaction kinetics of silver powder was not further investigated, due to the lower activity compared to the other inorganic catalysts.

RuO_2 shows the highest activity of the inorganic catalysts, PtNP(b1) shows the second highest, and MnO_2 the third highest activity. This is surprising, since platinum nanoparticles have previously been reported to have higher activity than RuO_2 [29] and catalase [38]. Dynamic light scattering measurements of MnO_2, RuO_2, and PtNP were performed to compare the particle size (see Fig. S1). The smaller size of RuO_2 compared to PtNP, might explain some of the deviation from literature. But, it should be noted that PtNP have a fibrous morphology [29], which increases the surface area. Furthermore, the different size of the two batches of PtNP might explain the difference in catalyst activity.

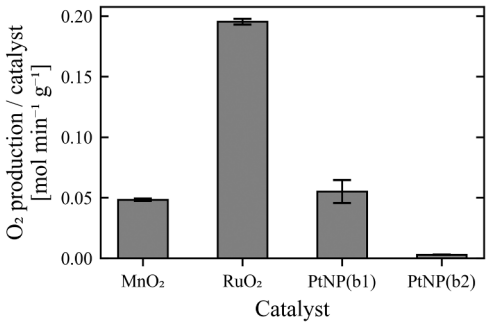

Fig. 2. Catalyst activity measurements at 50 mM H_2O_2 and 0.05 mg/mL catalyst. The slopes are obtained from linear regression of produced O_2 and divided with catalyst concentrations. The measurements are described in ESI. PtNP(b1) and PtNP(b2) are different synthesized batches of PtNP.

A great advantage of RuO_2 and MnO_2 over PtNP is their commercial availability. RuO_2 has a higher activity than MnO_2, and thus seems like the obvious choice of catalyst between these two. However, deciding between RuO_2 and PtNP is not straightforward. The different activities of different batches of PtNP show that the synthesis of the PtNP can be challenging, which is also indicated by the difference in size of the two batches of PtNP (Fig. S4-S5). Another important aspect is the signal intensity when the catalyst is immobilised in the sensor spot. The black colour of RuO_2 (Fig. S3) results in lower signal intensities. Therefore, it is possible to add three times the amount of PtNP (measured in mass) compared to RuO_2. Consequently, sensor foils prepared with RuO_2 and PtNPs show very similar production of O_2 when exposed to H_2O_2, see Fig. 3. We decided to use the batch of PtNPs with the highest activity, mainly because an additional conditioning step is necessary with RuO_2. This conditioning phenomena is further described in ESI (Fig. S6). However, we want to emphasize that RuO_2 can be a good alternative if no synthesis possibilities exist.

3.2. Removal of O_2 in the set-up

DO is removed from the analyte solution by passing it through silicon tubing submerged in the O_2 scavenging solution in the measurement set-up (Fig. 1A). The amount of oxygen removed is dependent on the residence time of the analyte solution in the silicone tubing. Therefore, it is intuitive to think that the pO_2 measured at the reference spot (at 0 H_2O_2) would decrease with slower flow rates. However, the minimum O_2 level in the cell is measured with flow rates 40 and 50 µL/min. At lower flow rates an O_2 ingress is evident, likely at the fluidic connections. Less O_2 is removed at higher flow rates, because of the lower residence time in the silicone tubing. An obvious solution to this would be to increase the length of the silicone tubing. Overall, the concentration of DO in the flow-through cell at all flow rates are low, and suitable for application of O_2 trace sensors.

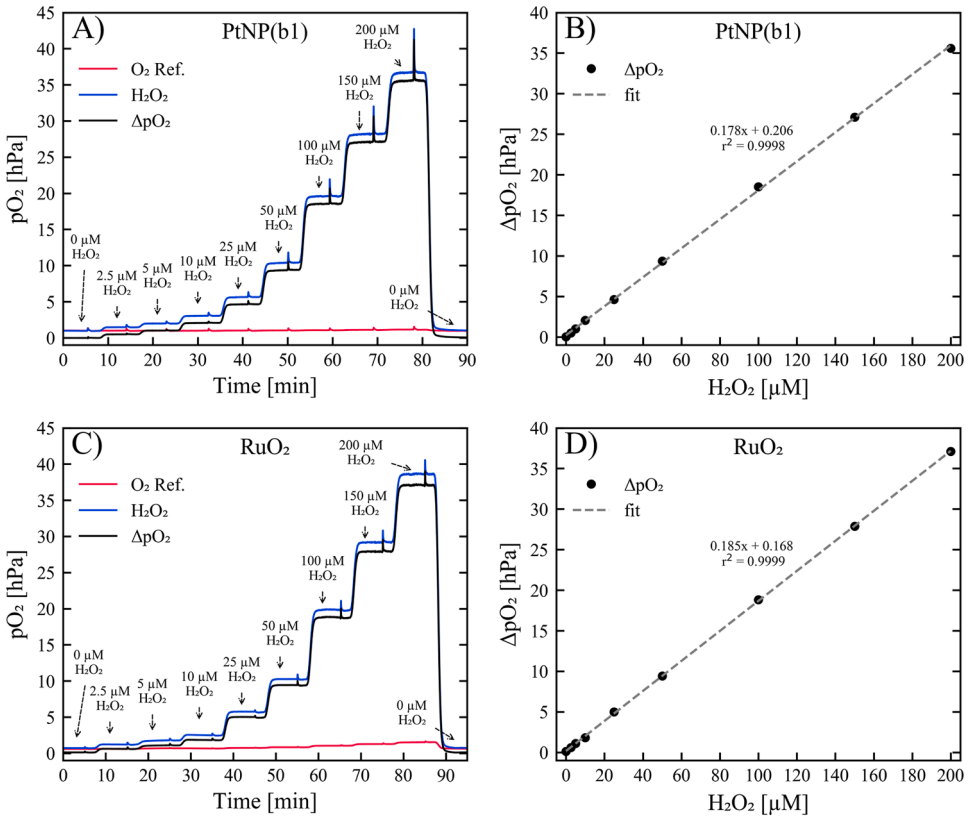

Fig. 3. A) and C) Response curve of the H_2O_2 sensor with PtNP(batch1) or RuO_2. 'O_2 ref.' (red line) is the amount of DO measured at the O_2 reference sensor spot, 'H_2O_2' (blue line) is the amount of O_2 measured at the H_2O_2 sensor spot, and 'ΔpO_2' (black line) is the difference between the two sensor spots and the amount of produced O_2. B) and D) The corresponding calibration curves with linear fits (grey, dotted line). The calibrations are performed at flow rate 50 µL/min with PdTPTBPF based sensor spots.

3.3. Response towards H_2O_2 and calibration

The sensor response time is a combination of the response time of the sensor spot and retention time. The latter is strongly influenced by the flow rate. The response times at different flow rates reported in Table 1 are the times from changing the analyte solutions until a stable signal is reached, and an average of each change of H_2O_2 solution. The total volume of the used set-up (from inlet to sensor spots) is approx. 135 µL.

The response of the sensor system towards H_2O_2 is shown in Fig. 3A, C. The spikes (e.g., at min 70 in Fig. 3A) are a result of stopping the flow to change H_2O_2 solutions and increases in pO_2 with higher H_2O_2 concentration. The sensor equilibrates within 5 min and is fully reversible. Sensor spots with RuO_2 show a slightly higher conversion of H_2O_2 mirrored in a higher detection of produced O_2 compared to PtNP containing spots. The difference in oxygen concentration (ΔpO_2) between the H_2O_2 spot and the O_2 reference spot is used in the calibrations (Fig. 3B,D). The H_2O_2 concentration is directly proportional to ΔpO_2 for both catalysts. However, the H_2O_2 is not fully converted. The slope of the calibration would be approx. 0.4 hPa/µM at full conversion, factoring in the stoichiometry of the degradation, at atmospheric pressure and room temperature. We assume that this difference is caused by diffusion limitations at the H_2O_2 sensor spot when measuring in flow. A temperature sensitive sensor foil was used to determine the temperature of the sample solution in the flow-through cell. This showed that the sample solution reaches room temperature in the deoxygenation set-up when the sample solution is between 4 °C and 24 °C at the inlet.

Table 1
Sensitivity/slope of calibration, response time (t_{100}), and baseline pO_2 at different flow rates. Response curves and calibration curves can be seen in Fig. S7–14.

Flow rate	Sensitivity/ Slope of calibration	Response time, t_{100}[a]	Baseline pO_2[b]
[µL/ min]	[ΔpO_2/µM]	[min]	[hPa]
10	0.187	18.7	3.55
20	0.176	10.6	1.52
30	0.188	7.1	1.13
40	0.182	5.4	0.93
50	0.179	4.6	0.93
60	0.172	4.2	1.37
70	0.165	3.5	2.16
80	0.162	3.2	3.30

[a] Response times are for the whole sensor system including retention time and sensor spot response.

[b] The baseline pO_2 is the amount of DO measured at the O_2 reference sensor spot in the flow-through cell with no H_2O_2 in the sample solution.

Measurements and calibrations with H_2O_2 concentrations 2.5–200 µM at flow rates between 10 and 80 µL/min are reported in the ESI (Figs. S8-S15). The sensitivities at different flow rates can be seen in Table 1. The general trend is that faster flow rates result in less sensitivity. Though, the change in sensitivity is smaller at the lower flow rates. We assume that the response is mainly limited by diffusion at the lower rates. In general, choosing the flow rate for the sensors is dependent on application, and the main considerations are sensitivity and response time. We chose a flow rate of 50 µL/min for further measurements.

3.4. Tuning of dynamic range

An important aspect of a sensor's application is the dynamic range. The use of PdTPTBPF allows to measure trace amounts of produced oxygen, which is suitable for low concentrations of H_2O_2. The LOD is

0.17 μM and 0.16 μM H_2O_2 for PtNP and RuO_2 containing spots, respectively. This is estimated from three times the signal standard deviation at 2.50 hPa, divided by the slopes of the calibrations seen in Fig. 3B,D. Previously, the best reported LOD is 15 μM H_2O_2 for similar concepts [29]. Whereas, electrochemical sensors have been reported to have LOD in the low nM range [19].

Fig. 4A shows a calibration between 0 and 10 μM H_2O_2 with good linearity. It can be seen that a concentration down to 1 μM can reliably be detected. Though, we theorise that even more sensitive O_2 sensors can be applied, if the measurement range is consistently in the very low H_2O_2 range. For instance, by changing the sensor matrix, as previously shown [23].

The resolution of PdTPTBPF based O_2 sensor decreases significantly at higher concentrations of DO. The dynamic range goes up to approx. 50 hPa, which corresponds to approx. 300 μM H_2O_2 with the calibrations shown in Fig. 4B. The sensor still has good linearity up to 500 μM H_2O_2, but it is recommended to use another O_2 indicator at this level of produced O_2. Therefore, we used a PtTPTBPF based sensor with PtNP catalyst as an example of measurements at higher H_2O_2 concentrations, and a calibration up to 1000 μM H_2O_2 can be seen in Fig. 4B.

3.5. Interferences and stability

The H_2O_2 calibrations in Fig. 3B,D and Fig. 4 have different sensitivity. This is likely caused by system-to-system variation when preparing sensor foils and the flow-through cells for measurements. Another system-to-system variation is the response of the O_2 reference sensor. Small amounts of O_2 are measured at the reference with increasing H_2O_2 concentrations (Fig. 3C, Fig. S16-S17). This is attributed to a diffusion of O_2 against the flow from the H_2O_2 spot to the O_2 ref. spot, thereby, affecting the ΔpO_2.

The sensor was tested for cross-sensitivities to sodium peroxynitrite (NaONOO), sodium hypochlorite (NaOCl), tert-butyl hydroperoxide (t-BuOOH), and ascorbic acid (A.A.), each at a concentration of 100 μM, and the responses are shown in Fig. 5. Overall, the tested species show

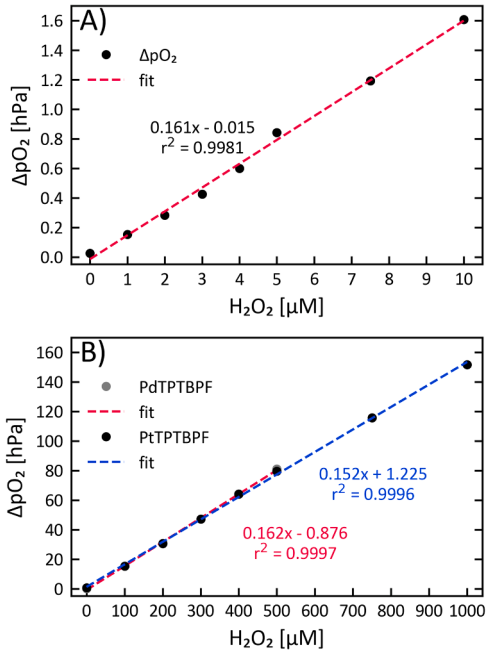

Fig. 4. A) H_2O_2 calibration at H_2O_2 concentration $\leq$ 10 μM. The calibration is performed with a PtNP and PdTPTBPF based sensor spot, at flow rate 50 μL/min. B) H_2O_2 calibration at H_2O_2 concentration $\leq$ 1000 μM. The calibrations are performed with PtNP and either PdTPTBPF or PtTPTBPF based sensor spots, at a flow rate of 50 μL/min. The corresponding response curves can be seen in Fig. S15-S17.

no or minor production of O_2 compared to H_2O_2 at same concentrations. The cross-sensitivities relative to H_2O_2 presented are NaONOO 2.7%, NaOCl 0.2%, t-BuOOH 0.1%, and ascorbic acid −2.2%. The sensor was further tested for cross-sensitivity to salinity of the sample solution by performing calibrations in 10 mM PBS and filtered sea water. The calibrations (Fig. S18) have similar slopes to the ones presented in Fig. 3, showing that the salinity does not affect the ability of the sensor to measure H_2O_2.

Another type of interference is from species that consume H_2O_2 by reaction before reaching the sensor spot. An example of such species is ascorbic acid, and the sensor response to even concentrations of freshly mixed H_2O_2 and ascorbic acid can be seen in Fig. 5. The interference is −11.7% at 100 μM of each. However, this is an intrinsic issue with the sensor, due to the retention time from the deoxygenation. Hence, increasing the flow rate of the measurement will reduce the time during which the species can react. This is further affected by the conditions of the measurement set-up, e.g. the temperature.

Hysteresis and stability of the sensor were tested by measuring alternating 20 and 100 μM H_2O_2 for a time period of 9 h, see Fig. 6. During this time, the sensor shows no hysteresis and good stability. ΔpO_2 decreases 0.7% and 0.6% at 20 and 100 μM H_2O_2, respectively. The measurement further shows that the sensor is fully reversible.

3.6. Production of H_2O_2 in GOx batch reactor

A model batch reactor was used to exemplify an application of the presented H_2O_2 sensor. GOx was immobilized in a batch reactor with O_2 bubbling to produce H_2O_2 from glucose. After conditioning, glucose is added (at timepoint 5 min), which initiates production of H_2O_2. This is measured with the sensor approx. 3 min later at timepoint 8 min, see Fig. 7. An assay with HRP and AR is used to verify the H_2O_2 concentrations. The assay measurements are in accordance with the concentrations measured by the sensor at 45 and 60 min, respectively, as can be seen in Fig. 7. The assay measures a slightly higher concentration of H_2O_2 at 110 min

4. Conclusion

We have presented a flow-based H_2O_2 sensor that uses O_2 as mediating species. Calibrations with sensor spots based on PdTPTBPF and either PtNP or RuO_2 show that both catalysts are suitable for the sensor, and produce sufficient amounts of O_2 to reliably measure between 1 and 200 μM H_2O_2. RuO_2 based sensors require an additional conditioning step, but are a good alternative to the PtNP, since RuO_2 is commercially available and does not require synthesis.

The dynamic range of the sensor can be extended to measure up to 1000 μM H_2O_2 with a PtTPTBPF based sensor at the cost of less sensitivity at the low H_2O_2 concentrations.

The sensor with PtNP was tested for interfering species, and show minor or no cross-sensitivities to NaONOO, NaOCl, t-BuOOH, and ascorbic acid at similar concentrations. The biggest cross-sensitivity was measured when mixing H_2O_2 and ascorbic acid, because the two species react and H_2O_2 is consumed before it reaches the sensor spot. This is a consequence of the retention time.

The sensor system has a high flow dependency, where mainly sensitivity and response time are affected. Both decrease as the flow rate increases. Commonly, the application defines the flow rate, and the sensor needs to be adapted accordingly. A possible adaption to the flow rate is the length of the silicone tubing used for deoxygenation, depending on the application it might be shortened to reduce retention time or elongated to ensure sufficient oxygen removal.

On the one hand, the sensor only works in flow, which can be problematic with small sample volumes. On the other hand, this makes it easy to integrated the sensor in fluidic/microfluidic applications, and enables continuous at-line sensing [39]. The materials are commercially available, making the sensor readily applicable, and the deoxygenation

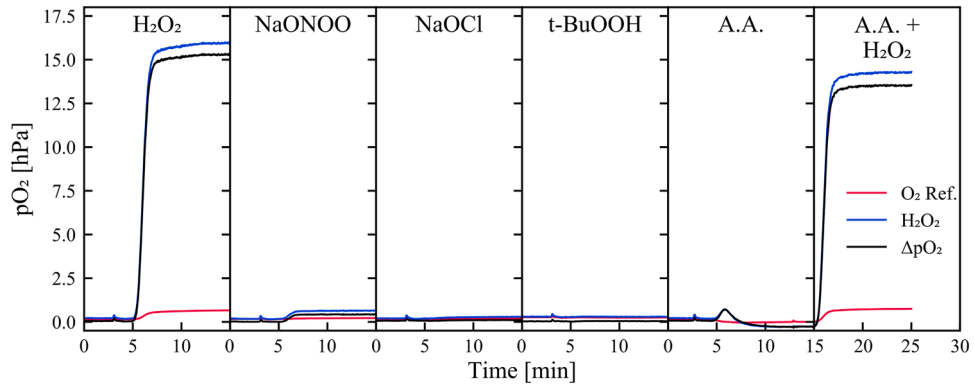

Fig. 5. Response of the sensor to 100 μM H_2O_2, 100 μM NaONOO, 100 μM t-BuOOH, 100 μM ascorbic acid (A.A.), and a freshly prepared mixture of 100 μM H_2O_2 and 100 μM ascorbic acid (A.A. + H_2O_2). The measurements are performed with PtNP as catalyst in the sensor spot and flow rate 50 μL/min. The legend applies to all measurements. 'O2 ref.' (red line) is the amount of DO measured at the O_2 reference sensor spot, 'H_2O_2' (blue line) is the amount of O_2 measured at the H_2O_2 sensor spot, and 'ΔpO_2' (black line) is the difference between the two sensor spots and amount of produced O_2.

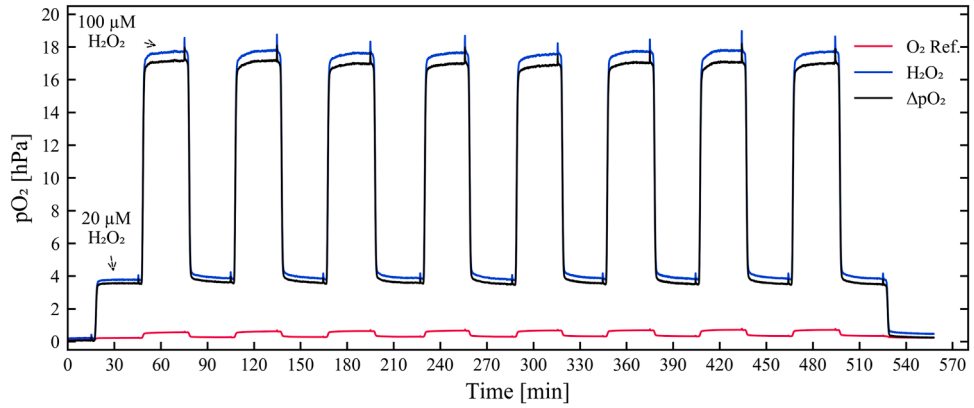

Fig. 6. Hysteresis and stability measured by alternating H_2O_2 concentration between 20 and 100 μM. 'O_2 ref.' (red line) is the amount of DO measured at the O_2 reference sensor spot, 'H_2O_2' (blue line) is the amount of O_2 measured at the H_2O_2 sensor spot, and 'ΔpO_2' (black line) is the difference between the two sensor spots and the amount of produced O_2. The measurement is performed at a flow rate of 50 μL/min with PdTPTBPF based sensor spots.

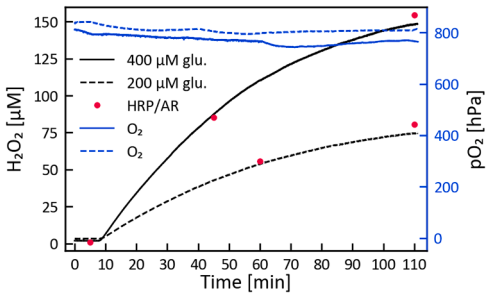

Fig. 7. Production of H_2O_2 in two separate experiments of a GOx and glucose based model batch reactor. Black lines are the concentration of H_2O_2 measured continuously with the reported H_2O_2 sensor at flow rate 50 μL/min. Red dots are sample concentration of H_2O_2 in the batch reactor measured with an HRP/AR assay. Blue lines are the concentration of DO in the model batch reactor measured with an O_2 microsensor.

is easy to set up.

At last, we showed that the sensor can be applied in a model batch reactor. For this, GOx was immobilized in a vial, and H_2O_2 was produced by adding glucose to the batch reactor. The measured values of H_2O_2 were validated with an HRP/AR assay, which showed good agreement between the two methods.

Overall, we developed a sensor that is capable of measuring H_2O_2 in fluidic applications with improved sensitivity compared to previous published methods.

CRediT authorship contribution statement

A.Ø.T. performed experiments, data analysis, and prepared the manuscript. B.J. contributed with experimental work. T.M. supervised the study, and prepare the manuscript. R.S.-A. and T.M. designed the flow-through cell. All authors have given approval to the final version of the manuscript.

Declaration of Competing Interest

The authors declare the following financial interests/personal relationships which may be considered as potential competing interests: T. M. is a founder, holds equity in PyroScience GmbH in Germany, and is the CEO of the Austrian branch, PyroScience AT GmbH. PyroScience is a developer, producer, and vendor of sensor technology.

Data availability

No data was used for the research described in the article.

Acknowledgment

This project has received funding from the European Union's Horizon 2020 research and innovation programme under the Marie

Skłodowska-Curie project No 812954.

Electronic supporting information

ESI contains the following: A complete list of chemicals and instrumentation, and images of sensor foils and measurement set-up. Synthesis of PtNP, and measurements of catalyst activity. Catalyst particle size measurements, and a description of an additional conditioning step necessary for RuO_2 based sensor spots. Calibrations at different flow rates and H_2O_2 concentrations.

Appendix A. Supporting information

Supplementary data associated with this article can be found in the online version at doi:10.1016/j.snb.2023.134904.

References

[1] A. Asghar, A.A. Abdul Raman, W.M.A. Wan Daud, Advanced oxidation processes for in-situ production of hydrogen peroxide/hydroxyl radical for textile wastewater treatment: a review, J. Clean. Prod. 87 (2015) 826–838, https://doi.org/10.1016/j.jclepro.2014.09.010.

[2] A.S. Stasinakis, Use of selected advanced oxidation processes (AOPs) for wastewater treatment - a mini review, Glob. NEST J. 10 (2008) 376–385, https://doi.org/10.30955/gnj.000598.

[3] B. Bissaro, A. Várnai, Å.K. Røhr, V.G.H. Eijsink, Oxidoreductases and reactive oxygen species in conversion of lignocellulosic biomass, Microbiol. Mol. Biol. Rev. 82 (2018) e00029–18, https://doi.org/10.1128/MMBR.00029-18.

[4] M. Hobisch, D. Holtmann, P. Gomez de Santos, M. Alcalde, F. Hollmann, S. Kara, Recent developments in the use of peroxygenases – exploring their high potential in selective oxyfunctionalisations, Biotechnol. Adv. 51 (2021), 107615, https://doi.org/10.1016/j.biotechadv.2020.107615.

[5] Z. Forsberg, M. Sørlie, D. Petrović, G. Courtade, F.L. Aachmann, G. Vaaje-Kolstad, B. Bissaro, Å.K. Røhr, V.G. Eijsink, Polysaccharide degradation by lytic polysaccharide monooxygenases, Curr. Opin. Struct. Biol. 59 (2019) 54–64, https://doi.org/10.1016/j.sbi.2019.02.015.

[6] R. Hage, A. Lienke, Applications of transition-metal catalysts to textile and wood-pulp, Angew. Chem. Int. Ed. 45 (2006) 206–222, https://doi.org/10.1002/anie.200500525.

[7] K.B. Beckman, B.N. Ames, The free radical theory of aging matures, Physiol. Rev. 78 (1998) 547–581, https://doi.org/10.1152/physrev.1998.78.2.547.

[8] T. Finkel, N.J. Holbrook, Oxidants, oxidative stress and the biology of ageing, Nature 408 (2000) 239–247, https://doi.org/10.1038/35041687.

[9] R.S. Balaban, S. Nemoto, T. Finkel, Mitochondria, oxidants, and aging, Cell 120 (2005) 483–495, https://doi.org/10.1016/j.cell.2005.02.001.

[10] B.C. Dickinson, C.J. Chang, Chemistry and biology of reactive oxygen species in signaling or stress responses, Nat. Chem. Biol. 7 (2011) 504–511, https://doi.org/10.1038/nchembio.607.

[11] W.M. Nauseef, How human neutrophils kill and degrade microbes: an integrated view, Immunol. Rev. 219 (2007) 88–102, https://doi.org/10.1111/j.1600-065X.2007.00550.x.

[12] E. Pick, Y. Keisari, A simple colorimetric method for the measurement of hydrogen peroxide produced by cells in culture, J. Immunol. Methods 38 (1980) 161–170, https://doi.org/10.1016/0022-1759(80)90340-3.

[13] M. Zhou, Z. Diwu, N. Panchuk-Voloshina, R.P. Haugland, A stable nonfluorescent derivative of resorufin for the fluorometric determination of trace hydrogen peroxide: applications in detecting the activity of phagocyte NADPH oxidase and other oxidases, Anal. Biochem. 253 (1997) 162–168, https://doi.org/10.1006/abio.1997.2391.

[14] M. Moßhammer, M. Kühl, K. Koren, Possibilities and challenges for quantitative optical sensing of hydrogen peroxide, Chemosensors 5 (2017) 28, https://doi.org/10.3390/chemosensors5040028.

[15] M. Moßhammer, V. Schrameyer, P.Ø. Jensen, K. Koren, M. Kühl, Extracellular hydrogen peroxide measurements using a flow injection system in combination with microdialysis probes – potential and challenges, Free Radic. Biol. Med. 128 (2018) 111–123, https://doi.org/10.1016/j.freeradbiomed.2018.05.089.

[16] P. Khan, D. Idrees, M.A. Moxley, J.A. Corbett, F. Ahmad, G. von Figura, W.S. Sly, A. Waheed, Md.I. Hassan, Luminol-based chemiluminescent signals: clinical and non-clinical application and future uses, Appl. Biochem. Biotechnol. 173 (2014) 333–355, https://doi.org/10.1007/s12010-014-0850-1.

[17] W. Chen, S. Cai, Q.-Q. Ren, W. Wen, Y.-D. Zhao, Recent advances in electrochemical sensing for hydrogen peroxide: a review, Analyst 137 (2012) 49–58, https://doi.org/10.1039/C1AN15738H.

[18] Z. Deng, L. Zhao, H. Zhou, X. Xu, W. Zheng, Recent advances in electrochemical analysis of hydrogen peroxide towards in vivo detection, Process Biochem 115 (2022) 57–69, https://doi.org/10.1016/j.procbio.2022.01.025.

[19] M.A. Riaz, Y. Chen, Electrodes and electrocatalysts for electrochemical hydrogen peroxide sensors: a review of design strategies, Nanoscale Horiz. 7 (2022) 463–479, https://doi.org/10.1039/D2NH00006G.

[20] J.P. Lowry, R.D. O'Neill, Homogeneous mechanism of ascorbic acid interference in hydrogen peroxide detection at enzyme-modified electrodes, Anal. Chem. 64 (1992) 453–456, https://doi.org/10.1021/ac00028a022.

[21] M. Schäferling, D.B.M. Grögel, S. Schreml, Luminescent probes for detection and imaging of hydrogen peroxide, Microchim. Acta 174 (2011) 1–18, https://doi.org/10.1007/s00604-011-0606-3.

[22] N.A. Burmistrova, O.A. Kolontaeva, A. Duerkop, New nanomaterials and luminescent optical sensors for detection of hydrogen peroxide, Chemosensors 3 (2015) 253–273, https://doi.org/10.3390/chemosensors3040253.

[23] K. Koren, L. Hutter, B. Enko, A. Pein, S.M. Borisov, I. Klimant, Tuning the dynamic range and sensitivity of optical oxygen-sensors by employing differently substituted polystyrene-derivatives, Sens. Actuators B 176 (2013) 344–350, https://doi.org/10.1016/j.snb.2012.09.057.

[24] X. Wang, O.S. Wolfbeis, Optical methods for sensing and imaging oxygen: materials, spectroscopies and applications, Chem. Soc. Rev. 43 (2014) 3666–3761, https://doi.org/10.1039/C4CS00039K.

[25] R. Zhang, W. Chen, Recent advances in graphene-based nanomaterials for fabricating electrochemical hydrogen peroxide sensors, Biosens. Bioelectron. 89 (2017) 249–268, https://doi.org/10.1016/j.bios.2016.01.080.

[26] H.E. Posch, O.S. Wolfbeis, Optical sensor for hydrogen peroxide, Microchim. Acta 97 (1989) 41–50, https://doi.org/10.1007/BF01197282.

[27] H.S. Voraberger, W. Trettnak, V. Ribitsch, Optochemical hydrogen peroxide sensor based on oxygen detection, Sens. Actuators B 90 (2003) 324–331, https://doi.org/10.1016/S0925-4005(03)00055-8.

[28] A. Mills, C. Tommons, R.T. Bailey, M.C. Tedford, P.J. Crilly, Reversible, fluorescence-based optical sensor for hydrogen peroxide, Analyst 132 (2007) 566, https://doi.org/10.1039/b618506a.

[29] L. Ding, S. Chen, W. Zhang, Y. Zhang, X. Wang, Fully reversible optical sensor for hydrogen peroxide with fast response, Anal. Chem. 90 (2018) 7544–7551, https://doi.org/10.1021/acs.analchem.8b01159.

[30] M. Quaranta, S.M. Borisov, I. Klimant, Indicators for optical oxygen sensors, Bioanal. Rev. 4 (2012) 115–157, https://doi.org/10.1007/s12566-012-0032-y.

[31] O.S. Wolfbeis, Luminescent sensing and imaging of oxygen: fierce competition to the Clark electrode, BioEssays 37 (2015) 921–928, https://doi.org/10.1002/bies.201500002.

[32] Y. Wei, Y. Jiao, D. An, D. Li, W. Li, Q. Wei, Review of dissolved oxygen detection technology: from laboratory analysis to online intelligent detection, Sensors 19 (2019) 3995, https://doi.org/10.3390/s19183995.

[33] S.M. Borisov, G. Nuss, I. Klimant, Red light-excitable oxygen sensing materials based on platinum(II) and palladium(II) benzoporphyrins, Anal. Chem. 80 (2008) 9435–9442, https://doi.org/10.1021/ac801521v.

[34] B. Nacht, C. Larndorfer, S. Sax, S.M. Borisov, M. Hajnsek, F. Sinner, E.J.W. List-Kratochvil, I. Klimant, Integrated catheter system for continuous glucose measurement and simultaneous insulin infusion, Biosens. Bioelectron. 64 (2015) 102–110, https://doi.org/10.1016/j.bios.2014.08.012.

[35] S. Kreß, R. Schaller-Ammann, J. Feiel, J. Wegener, J. Priedl, W. Dietrich, C. Kasper, D. Egger, Innovative platform for the advanced online monitoring of three-dimensional cells and tissue cultures, Cells 11 (2022) 412, https://doi.org/10.3390/cells11030412.

[36] S.M. Borisov, G. Nuss, W. Haas, R. Saf, M. Schmuck, I. Klimant, New NIR-emitting complexes of platinum(II) and palladium(II) with fluorinated benzoporphyrins, J. Photochem. Photobiol. A 201 (2009) 128–135, https://doi.org/10.1016/j.jphotochem.2008.10.003.

[37] B. Brena, P. González-Pombo, F. Batista-Viera, Immobilization of Enzymes: A Literature Survey, in: J.M. Guisan (Ed.), Immobilization of Enzymes and Cells, Third edition, Humana Press, Totowa, NJ, 2013, pp. 15–31, https://doi.org/10.1007/978-1-62703-550-7_2.

[38] Z. Zhu, Z. Guan, D. Liu, S. Jia, J. Li, Z. Lei, S. Lin, T. Ji, Z. Tian, C.J. Yang, Translating molecular recognition into a pressure signal to enable rapid, sensitive, and portable biomedical analysis, Angew. Chem. Int. Ed. 54 (2015) 10448–10453, https://doi.org/10.1002/anie.201503963.

[39] P. Gruber, M.P.C. Marques, N. Szita, T. Mayr, Integration and application of optical chemical sensors in microbioreactors, Lab Chip 17 (2017) 2693–2712, https://doi.org/10.1039/C7LC00538E.

Anders Ø. Tjell holds a MSc in Chemistry from Aalborg University (Denmark), Department of Chemistry and Bioscience. He is currently a Ph.D. student at the Institute of Analytical Chemistry and Food Chemistry at the Graz University of Technology. His research focuses on development, fabrication, and integration of optical sensors in microfluidic applications.

Barbara Jud is studying Biomedical Engineering at the Graz University of Technology. She is currently working on her master's thesis at the Institute of Analytical Chemistry and Food Chemistry. Her work revolves around optical hydrogen peroxide sensors in applications relevant to bioreactors.

Roland Schaller-Ammann is a researcher at JOANNEUM RESEARCH – Institute for Biomedical Research and Technologies since 2004. He received his Ph.D. in biomedical engineering from the University of Graz (Austria) in 2010. In 2010–2018 he was a post-doctoral fellow. Since 2018 he is senior scientist in the same institute. His research interests include, design and development and certification of biomedical devices, namely OFM (open flow microperfusion), pre-clincical and clinical studies, drug development including pharmacokinetics (PK) and pharmacodynamics (PD), biosensors, lab-on-chip systems, and micro-bioreactors.

Torsten Mayr received his Ph.D. in chemistry from the University of Regensburg (Germany) in 2004. In 2002–2004 he was a post-doctoral fellow at the Karolinska Institute in Stockholm (Sweden). Since 2004 he is assistant professor at the Institute of Analytical Chemistry and Food Chemistry at the Graz University of Technology. Since 2014 he is Associate Professor the same institute. His research interests include optical chemical sensors, biosensors, functionalized micro- and nanoparticles, flow chemistry, lab-on-chip systems, micro-bioreactors and organ-on-chips.